

# Split Time Method for the Probabilistic Characterization of Stability Failures in Quartering Seas

Vadim Belenky

(David Taylor Model Basin / NSWCCD, Maryland, USA)

Kostas Spyrou

(National Technical Institute of Athens, Greece)

Kenneth M. Weems, Woei-Min Lin

(Science Applications International Corporation, Bowie, Maryland, USA)

## ABSTRACT

This paper describes recent progress and issues in the development of the split time method for predicting the probability of a roll motion stability failure – capsize or extreme roll motion event – for a ship operating in irregular ocean waves. The split time method attempts to address the challenge presented by the rarity and physical complexity of such events separating the problem into a sequence of non-rare and rare problems that can be practically characterized with advanced numerical methods. In the broadest terms, the non-rare problem can be described as determining the rate of occurrence of an intermediate event such as the upcrossing of a threshold roll angle, while the rare problem can be described as determining the probability of capsizing when this intermediate event is realized. The current development of the method focuses on two areas related to the application of this method for nonlinear ship motion in quartering seas.

The first area of development is the variation of the ship's roll restoring curve in following or quartering seas, which is a key element in a pure loss of stability event. To incorporate this phenomenon, the split time method has been reformulated with the intermediate roll threshold and the critical roll rate leading to capsizing after upcrossing described by stochastic processes. The implementation of this method with the results of numerical simulation data has led to several important results, including the understanding that roll and roll rates may be dependent processes in quartering seas and the development of novel procedure for characterizing distribution of the dependent process at the instant of upcrossing.

The second area of development is the probabilistic model of surf-riding, which is a necessary step toward evaluating the probability of capsizing or large roll motion due to broaching-to following surf-riding. Recent results include the evaluation of a suitable wave celerity in irregular seas and the use of the existence or non-existence of surf-riding equilibria to describe a ship's transition into and out of surf-riding.

## INTRODUCTION

### *The Challenge*

Since an extreme roll motion event can result in severe damage to or even the loss of a ship, a physics-based evaluation of the probability of such a stability failure in severe irregular seas would be a very useful measure for the assessment of operational risk. This is especially true for novel or unconventional designs, where operational experience is insufficient or even non-existent.

The principal challenge to the development and implementation of such an evaluation is a combination of the nonlinearity and rarity of such events. Large roll angles are associated with significant nonlinearity of the roll restoring (GZ) curve while capsizing, as a transition between two stable equilibria, is the ultimate manifestation of nonlinearity. Furthermore, there are a number of different scenarios of stability failure. Dynamics of capsizing in beam seas is straight forward and, in principle, is similar to an escape from a potential well. Following and stern quartering seas lead to random stiffness due to the change of the roll restoring curve in waves and more complex behavior. Surf-riding and broaching-to lead to even more complex dynamics, involving surf-riding equilibria and lateral motions.

On the other hand, a stability failure of an intact ship is very rare, even in severe operational conditions. As a result, a direct application of a Monte Carlo approach using advanced simulation tools becomes computationally costly and ineffective, while the severe nonlinearity precludes the use of simpler dynamic models. A direct fitting of an extreme value distribution is also problematic, as such fitting is a statistical procedure and the result will be defined by the statistically dominant data in the sample. The small-amplitude motions are generally statistically dominant and their physics is different from large motions because of nonlinearity, so the extreme value distribution would not reflect the physics of large-amplitude motions.

## The Principle of Separation and Piecewise Linear System

One promising way to solve this problem is the application of the Principle of Separation (Belenky *et al.* 2012), in which different solutions are considered for domains with different physics. The split time method is one manifestation of this principle. The simplest illustration (and earliest application) of the Principle of Separation is based on a rudimentary model of roll with a piecewise linear presentation of the nonlinear GZ curve, as shown in Figure 1.

In this presentation, the different linear ranges correspond to different physics: attractors or repellers. This sequence of attractors and repellers allows the modeling of a transition between two stable equilibria, which is the essence of a capsizing. The probability of at least one capsizing during time  $T$  can be expressed as

$$P(T) = 1 - \exp(-\xi P_C T) \quad (1)$$

Here  $\xi$  is an upcrossing rate through the boundary between the range 0 and range 1, while  $P_C$  is the probability of capsizing after the upcrossing.

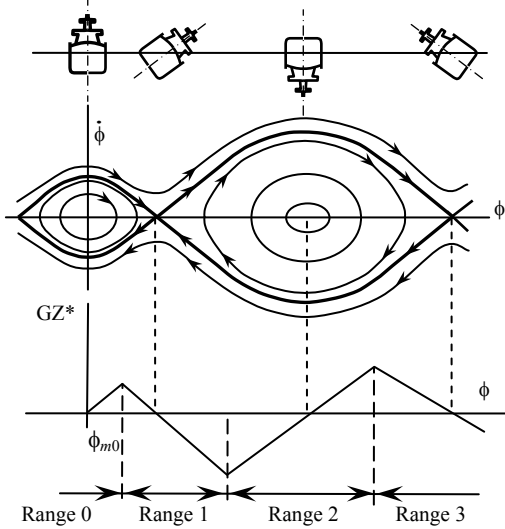


**Figure 1:** Modeling Severe Nonlinearity with Piecewise Linear Stiffness (Belenky, 1993)

Formula (1) is the basis for expressing the Principle of Separation in which the problem is separated into non-rare and rare problems. The probability of capsizing after upcrossing  $P_C$  is the objective for the rare problem, while the upcrossing rate  $\xi$  is targeted by the non-rare problem formulation.

Since the upcrossings are relatively rare, the statistics of the roll response (in the absence of capsizing) will not be significantly affected by the upcrossings themselves. As a result, the processes of roll angles and rates can be assumed to be normal. The upcrossing rate is then available in closed-form:

$$\xi = \sqrt{\frac{V_{\dot{\phi}}}{V_{\phi}}} \exp\left(-\frac{\phi_{m0}^2}{2V_{\phi}}\right) \quad (2)$$

Here  $V_{\dot{\phi}}$  is the variance of roll, while the dot above the symbol stands for the temporal derivative. Since the system is linear within Range 0, the variances of both roll and roll rate are available from the frequency domain solution.

The conditions of capsizing after upcrossing are formulated through the initial conditions at the instant of upcrossing. It has been shown that the roll rate at the instant of upcrossing has a dominant influence on the results (Belenky 1993), so the condition of capsizing after upcrossing can be expressed as an exceedance of a critical roll rate:

$$P_C = P(\dot{\phi}_c > \dot{\phi}_{cr}) = \int_{\dot{\phi}_{cr}}^{\infty} f_c(\dot{\phi}) d\dot{\phi} \quad (3)$$

Here index “cr” stands for “critical” and the index “c” indicates “at the instant of upcrossing”. The probability density function (PDF)  $f_c$  is different from the general distribution of roll rates, because the instant of upcrossing is not just “any instant of time”. This leads to a general problem of the distribution of a derivative at the instant of upcrossing. In the general case, it can be expressed through a joint distribution of roll angles and rates (Belenky *et al.* 2008, 2010):

$$f_c(\dot{\phi}_c) = \frac{\dot{\phi}_c f(\phi = \phi_{m0}, \dot{\phi}_c)}{\int_0^{\infty} \dot{\phi} f(\phi = \phi_{m0}, \dot{\phi}) d\dot{\phi}} \quad (4)$$

For the piecewise linear system, both roll angles and rates are uncorrelated normal processes, so the distribution (4) is actually a Rayleigh distribution.

$$f_c(\dot{\phi}_c) = \frac{\dot{\phi}_c}{V_{\dot{\phi}}} \exp\left(-\frac{\dot{\phi}_c^2}{2V_{\dot{\phi}}}\right) \quad (5)$$

The verification of the Rayleigh distribution by numerical simulation has been presented in Belenky *et al.* (2008). The dynamical system with piecewise linear stiffness also allows a closed form expression for the critical roll rate.

$$\dot{\phi}_{cr} = \lambda_2 (\phi_{m0} - \phi_v) \quad (6)$$

Here  $\phi_v$  is the angle of vanishing stability and  $\lambda_2$  is a negative eigenvalue of the linear solution for the repeller in Range 1:

$$\lambda_2 = -\delta - \sqrt{\omega_0^2 k_{f1} + \delta^2} \quad (7)$$

$k_{f1}$  is the angle coefficient of stiffness in Range 1, expressed in terms of the roll natural frequency  $\omega_0$ , while  $\delta$  is the roll damping coefficient. Belenky, *et al.* (2008) reported a successful convergence test for the

piecewise linear system, in which the theoretical solution was verified with numerical simulation.

The piecewise linear system is, quite possibly, the simplest model of capsize, and is most useful for formulating potential solutions of the problem. However, for a realistic assessment, a model that is more representative of the true hull shape is needed. Nevertheless, it has found its applications (Iskandar and Umeda 2001, Paroka and Umeda 2006, Umeda, *et al.*, 2007, 2011).

### The Principle of Separation and the Split-Time Method

The simplicity of the piecewise linear model of roll has helped towards understanding how to simultaneously deal with the nonlinearity and rarity of capsizing and has helped to formulate the Principle of Separation. Further development has led to the split-time method, in which a numerical simulation is used instead of the solution of the linear differential equation.

Belenky, *et al.* (2008) describes the application of the time-split method for the case of beam seas, which is illustrated in Figure 2. The non-rare problem is the estimation of the rate of upcrossing of the angle of the maximum of the GZ curve and the distribution of the roll rate at the instant of upcrossing. It can be solved numerically using an advanced hydrodynamic simulation code, providing a more accurate solution that a frequency domain and incorporating exact nonlinear restoring.

The rare problem can also be solved numerically using a series of short simulation starting from the threshold roll angle with different initial roll rates. The critical roll rate is found by an iterative process which is illustrated in the inset of Figure 2.

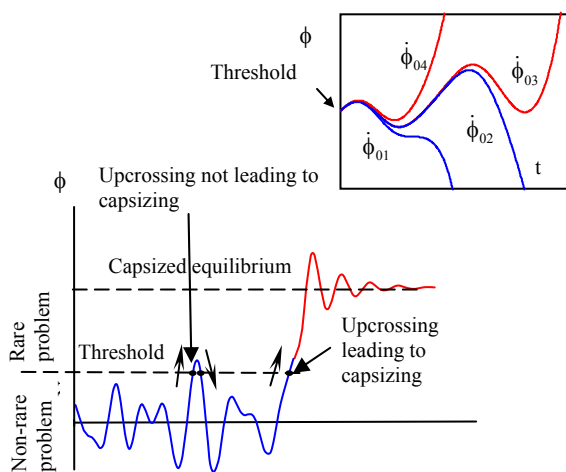


**Figure 2** Concept of Split-Time Method for Capsizing in Beam Seas (Belenky, *et al.* 2008)

The method has been implemented using the Large Motion Program (LAMP), but can, in principal, be used with any time domain simulation code. One of the significant consequences of using time domain simulation is statistical uncertainty, since all the outputs of the Monte-Carlo method are random numbers. The implementation of the method incorporates the idea that a confidence interval of each statistical estimate can be evaluated for each step of the process and propagated through the final result (Belenky and Weems 2008). The tumblehome and flared configurations of the ONR Topsides series (Bishop, *et al.*, 2005) were used for a set of sample capsizing probability calculations which are also described in Belenky, *et al.*, (2008).

### Split-Time Method for Random Stiffness

The next step of the development of the split-time method was the consideration of the variation of roll restoring characteristics in stern quartering and following seas, which is realized as random stiffness. To include the random stiffness, the upcrossing threshold roll angle and the critical roll rate are now considered to be stochastic processes. The general scheme, nevertheless, remains the same, as illustrated in Figure 3:

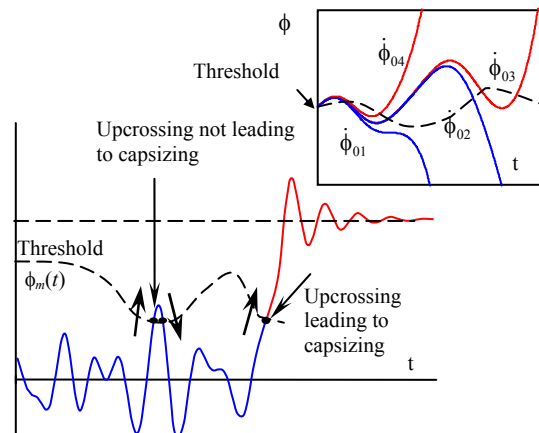


**Figure 3** Concept of Split-Time Method Generalized for Stability Variation in Waves (Belenky *et al.* 2010).

Since the threshold is a stochastic process, it is convenient to introduce a so-called “carrier” process representing the instantaneous difference between the threshold roll angle and the instantaneous roll angle:

$$x(t) = \phi(t) - \phi_m(t) + \phi_{m0} \quad (8)$$

Here  $\phi_m(t)$  is the threshold roll angle at time  $t$ , which is set to be in the vicinity of, but not necessarily at, the angle of the maximum of the GZ curve. Belenky *et al.* (2010) describes an algorithm for setting a threshold roll angle which preserves the separation of the

problem will while maintaining the differentiability of the carrier process, even for cases where the instantaneous restoring curve becomes degenerate.

The critical roll rate is also a random process and must be calculated at each instant of time, and its solution must consider the continuing variation of the roll restoring after upcrossing. It is convenient to define a process of the difference between the instantaneous and critical roll rates;

$$y(t) = \dot{\phi}_{cr}(t) - \dot{\phi}(t) \quad (9)$$

The process  $y(t)$  and the process  $x(t)$  are dependent (Belenky *et al.* 2010). The definition of these two processes allows formula (1) to be used for probability of capsizing, but with the upcrossing defined for the carrier process  $x(t)$  rather than the roll angle  $\phi$ . Using the general formula for the upcrossing rate:

$$\xi = \int_0^{\infty} f(x = \phi_{m0}, \dot{x}) d\dot{x} \quad (10)$$

The probability of capsizing after upcrossing is expressed as:

$$P_C = \int_{-\infty}^0 f_c(y_c) dy_c \quad (11)$$

The probability density distribution  $f_c$  refers to the values of the process  $y(t)$  taken at the instant when the process  $x(t)$  up-crosses the level  $\phi_{m0}$ . This leads to the general problem of the distribution of a dependent process at the instant of upcrossing. In the general case, it can be expressed through joint distribution of the process, its derivative and the dependent process (Belenky *et al.* 2010):

$$f_c(y_c) = \frac{\int_0^{\infty} \dot{x} f(x = \phi_{m0}, \dot{x}, y_c) d\dot{x}}{\int_0^{\infty} \dot{x} f(x = \phi_{m0}, \dot{x}) d\dot{x}} \quad (12)$$

Formula (12) has been verified by numerical simulation using a process of wave elevations and derivative. The dependent process was simulated by introducing a phase shift into the Fourier series presentation of the wave elevations (Belenky *et al.* 2010)

To test the concept, a piecewise linear system with variable stiffness was considered. The decreasing part of the stiffness is assumed to be randomly shifting parallel to calm water value, simulating the stability variation in waves, see Figure 4. All of the elements of this random stiffness have normal distribution. The dynamical system with varying piecewise linear stiffness shown in Figure 4 allows a closed form solution for the capsizing probability. The convergence of the solution has been verified using Monte-Carlo simulations (Belenky *et al.* 2010, 2011).

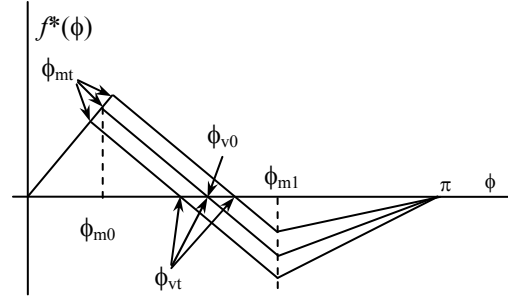


**Figure 4:** Piecewise Linear Stiffness Term with Time-Varying Decreasing Part (Belenky *et al.* 2010)

The numerical implementation of the split-time method with random stiffness requires a time-domain evaluation of the stability variation in waves, which has been implemented in LAMP (Belenky and Weems 2008a, Belenky *et al.* 2010). At each time step of the simulation, the wave surface is “frozen”, the ship is rotated through a range of incremental heel angles about its instantaneous position on the wave, and the resultant righting moment is calculated from the change in the body-nonlinear hydrostatic and Froude-Krylov pressure forces, see Figure 5.

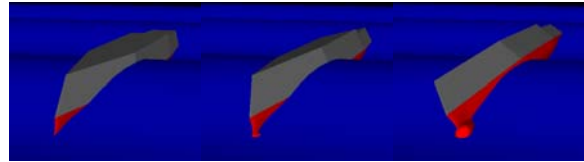


**Figure 5** Applying Incremental Heeling Angles to the ONR Topsides Tumblehome Hull Form for the Calculation of the GZ Curve in Waves (Belenky *et al.* 2010)

The further numerical implementation of the split-time method has encountered some difficulties. It is well known and has been formally proven that a stationary stochastic process and its first derivative are not correlated (*e.g.* Priestley, 1981). Usually, the absence of correlation is considered as a good basis for assuming independence. Numerical simulations, however, show that the assumption of independence is not applicable for the carrier process in stern-quartering waves. This problem is considered in more detail later in this paper.

### ***Split-Time Method for Surf-riding and Broaching-to***

A probabilistic description of stability in stern-quartering and following seas cannot be completed without the consideration of broaching-to, which, along with pure loss of stability, provides one of the principal mechanisms for capsizing or attaining a large roll angle. The nature of broaching-to in regular waves is now well understood using concepts from

nonlinear dynamics (Spyrou 1996, 1997). In general, two distinct mechanisms of broaching-to are identified.

The first mechanism is broaching-to preceded by surf-riding, which is a dynamic equilibrium along the ship's longitudinal axis in which the ship is accelerated to the speed of the wave. While being stable in surge, this equilibrium can be (depending on the effectiveness of the applied control action) unstable in yaw direction, forcing the ship into an uncontrollable and sometimes violent turn. Such a turn can be accompanied by a large roll angle caused by centrifugal forces and may eventually result in capsize. The second mechanism of broaching-to is more relevant to larger ships and it involves a resonant-type escape from the intended course. Some types of control may create a hysteresis in yaw with two stable modes existing at the same time. The broaching-to of that type is associated with a fold bifurcation in yaw.

As with the previous work, the initial numerical code development and implementation of the split-time method for surf-riding and broaching-to is being based on the LAMP code. Prior to attempting the development of a probabilistic description of broaching-to, a study was performed in order to verify that the hydrodynamic code is capable of reproducing known surf-riding and broaching-to behavior. A sample result from this study is shown in Figure 6, where the co-existence of surf-riding and periodic surging responses for different initial condition in the same regular wave is demonstrated.

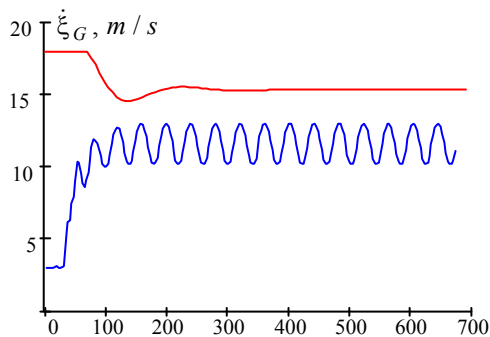


**Figure 6** LAMP Modeling of Coexistence of Surging and Surf-riding.

The study, which is presented in Spyrou, *et al.* (2009) and summarized in Belenky *et al.* (2010), has demonstrated that most of the known surf-riding and broaching-to dynamics can be reproduced with the code. This result clears the way for the development and implementation of a probabilistic consideration of stability failures caused by broaching-to using the split-time method and the results of numerical simulation. The further development is described below in this paper.

## STATISTICS OF ROLL IN STERN-QUARTERING SEAS

### Unexpected Results for Upcrossing Rate in Stern-Quartering Seas

As mentioned above, the absence of correlation between two random processes is usually considered as a basis for assuming independence, allowing the formula (10) for the upcrossing rate to be simplified:

$$\xi = f(x = \phi_{m0}) \int_0^{\infty} \dot{x} f(\dot{x}) d\dot{x} \quad (13)$$

While verifying the numerical implementation of the split-time method, the upcrossing rate was estimated by direct counting and compared to the results of formula (13) using different models for the distribution of the derivative of the carrier. The result was unexpected; the confidence interval of the estimated upcrossing rate did not contain the value calculated using formula (13). The same result was obtained when the comparison was made for roll angles. At the same time, an application of formula (10) without assuming independence gave reasonable agreement, as shown in Figure 7.

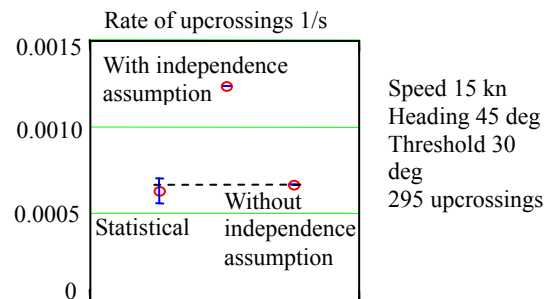


**Figure 7** Observed and Predicted Rate of Upcrossing for Roll Angle: Speed 15 kn (Belenky *et al.* 2010)

In order to check the sensitivity of these results to the specifics of the calculation, the numerical simulations and upcrossing rate comparison was repeated for two additional conditions: a quartering sea condition in which speed was changed by 1 knot and the heading by 5 degrees, and beam seas. The results for the second quartering sea condition were very similar to the first. For the beam case, however, the statistical estimate agreed with both formulae (10) and (13), see (Belenky *et al.* 2010). The results suggest that roll and roll rate may be dependent in stern quartering seas, even while they may appear to be independent in beam seas. The principal difference between these conditions is the variation of the roll restoring in waves, which will be generally be small in beam seas (at least in long-crested beam seas) but will be large in

quartering and following seas. The conclusion is that the dependence of the roll and roll rate may be a result of a change in the physics of rolling due to this change in the roll restoring characteristics

### Model of Joint Distribution

The methods for modeling probability density function (PDF) described in Belenky and Weems, (2008) and Belenky *et al.* (2008) did not include models for joint distributions, which is needed for formula (10). A simple model for a joint PDF was developed based on the moving average algorithm applied to a histogram. This approach takes advantage of the large number of data points in the stochastic process.

The calculation scheme is as follows. Consider two stochastic processes  $x$  and  $z$  presented with sets of time histories. The first step is the calculation of the estimate of conditional variance of the process  $x$  under the condition that the process  $z$  takes a particular value. The second step is the evaluation of a series of conditional histograms. Then the conventional “boxcar” formula is applied to each of the conditional histograms. The result is actually a model of conditional PDF of the processes  $x$  and  $z$ . To complete the calculation, the same procedure is applied to marginal histogram of process  $z$ . Finally, an approximate PDF, denoted by the symbol  $f^*$ , is computed as:

$$f^*(x, z) = f^*(x|z)f^*(z) \quad (14)$$

This procedure does not guarantee satisfaction of the normalization conditions or equality of variance, so corrections are necessary as described in Belenky and Weems (2008). Figure 8 shows the sample of a joint PDF computed for the wave elevations (process  $x$ ) and its derivatives (process  $z$ ). The result is visually very similar to joint PDF of two uncorrelated Gaussian processes. More details on the method are available in Belenky and Weems (2012a).

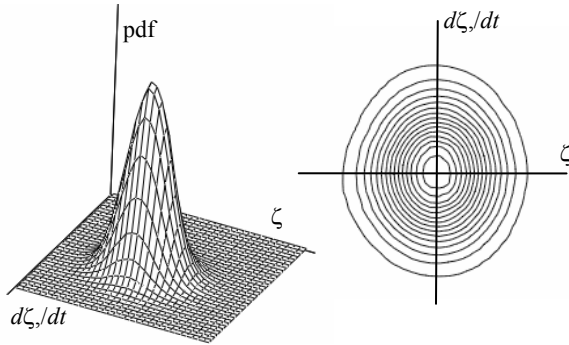


**Figure 8** Joint PDF and Horizontal Section for Wave Data (Belenky and Weems, 2012a).

### Estimates of Correlation

A correlation is a measure of the dependence between two random variables or stochastic processes. It is expressed through the covariance, which is the second joint central moment. For stochastic processes of roll angles and rates presented with an ensemble of  $N_r$  records of  $N_t$  point each, its estimate is expressed as:

$$M^*[\phi, \dot{\phi}] = \frac{\sum_{j=1}^{N_r} \sum_{i=1}^{N_t} (\phi_{i,j} - m_\phi^*) \dot{\phi}_{i,j}}{N_t N_r} \quad (15)$$

Here the asterisk means “estimate” and  $m_\phi$  stands for mean value of roll angle. The estimate of the correlation coefficient is expressed as

$$r^*[\phi, \dot{\phi}] = \frac{M^*[\phi, \dot{\phi}]}{\sqrt{V_\phi^* V_{\dot{\phi}}^*}} \quad (16)$$

It is normalized by the standard deviations and changes from -1 to 1.

Independent variables or processes are not correlated, but the opposite is not always correct; dependent processes may be uncorrelated. Only normal processes (or variables) are guaranteed to be independent when they are uncorrelated. It has been proven formally that the first derivative of a stationary stochastic process is not correlated with the process itself. Therefore, the objective of this statistical analysis here is to verify the calculation method (especially confidence interval) against theoretical values.

Four data sets are used for a numerical study of this problem. The first is a wave elevation data set (Belenky and Weems 2012a) while the other three are roll motion data sets from LAMP simulations (Belenky *et al.* 2010). The roll motion data sets are for two stern quartering conditions (heading 45 and 40 degrees with speed 15 and 14 kn respectively) and one beam seas conditions. The wave elevation data set consists of 200 records of 30 minutes duration while the ship motion data sets consist of 200 records of 40 minutes duration.

Since the volume of the sample is large, normal distribution was assumed for the estimates of covariance (15) and correlation coefficient (16). Following Priestley (1981) the variance of the covariance estimate for a record was estimated as:

$$V_R(M_{\phi, \dot{\phi}}^*) = \frac{1}{N_t - k} \sum_{i=-N_t+k+1}^{N_t-k-1} \left(1 - \frac{|i|}{N_t}\right) \times (R_\phi^*(t_{|i|})R_{\dot{\phi}}^*(t_{|i|}) + R_{\phi, \dot{\phi}}^*(t_i)R_{\dot{\phi}, \phi}^*(t_i)) \quad (17)$$

Here  $R_\phi^*$  and  $R_{\dot{\phi}}^*$  are estimates of the autocorrelation functions of roll angles and rates, respectively, while

$R_{\phi, \dot{\phi}}^*$  is an estimate of the cross-correlation function for roll and roll rates. The variance of the covariance for the ensemble is expressed as:

$$V(M_{\phi, \dot{\phi}}^*) = \frac{1}{N_R^2} \sum_{j=1}^{N_R} V_{Rj}(M_{\phi, \dot{\phi}}^*) \quad (18)$$

Details of calculation of these estimates can be found in Belenky and Weems (2012a). The result of statistical processing of these data samples in terms of correlation coefficients is shown in Figure 9. Confidence probability was accepted to be 95%. All of the confidence intervals contain zero, so the statistical technique is not rejected by the theory.

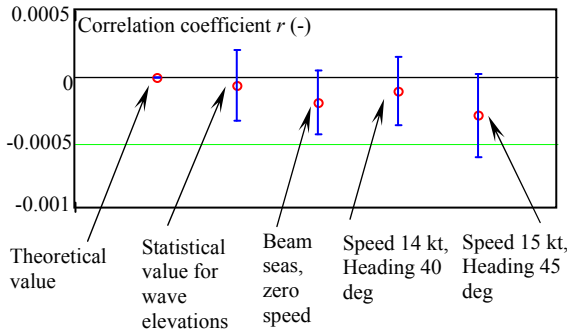


**Figure 9:** Estimates of Correlation Coefficients between the Processes and Derivatives (Belenky and Weems 2012a)

### Correlation of Higher Order

Since the correlation between the roll and roll rates is zero, the measure of dependence should be searched in higher-order joint moments. The estimate of the second joint central moment – the second-order covariance is expressed as:

$$M2^*[\phi, \dot{\phi}] = \frac{\sum_{j=1}^{N_r} \sum_{i=1}^{N_t} (\phi_{i,j} - m_\phi)^2 (\dot{\phi}_{i,j})^2}{N_t N_r} \quad (19)$$

An estimate for non-dimensional second-order correlation coefficient is written as:

$$r2^*[\phi, \dot{\phi}] = \frac{M2^*[\phi, \dot{\phi}]}{V_\phi^* V_{\dot{\phi}}^*} \quad (20)$$

The calculation of both of these estimates from the time series is straight forward. It is not difficult to see that if the processes are independent, the second order correlation coefficient will equal unity:

$$r2 = \frac{1}{V_\phi V_{\dot{\phi}}} \int \int_{-\infty}^{\infty} f(\phi, \dot{\phi}) (\phi - m_\phi)^2 \dot{\phi}^2 d\phi d\dot{\phi} = \quad (21)$$

$$\frac{1}{V_\phi V_{\dot{\phi}}} \int_{-\infty}^{\infty} f(\phi) (\phi - m_\phi)^2 dx \int_{-\infty}^{\infty} f(\dot{\phi}) \dot{\phi}^2 d\dot{\phi} = \quad (21)$$

$$\frac{V_\phi V_{\dot{\phi}}}{V_\phi V_{\dot{\phi}}} = 1$$

To evaluate the statistical uncertainty, the second-order covariance can be expressed through the first order covariance of the centered squares of roll and roll rates:

$$M2^*[\phi, \dot{\phi}] = M^*[\phi2, \dot{\phi}2] + V_\phi^* V_{\dot{\phi}}^* \quad (22)$$

where the centered squares are:

$$\phi2 = (\phi - m_\phi)^2 \quad ; \quad \dot{\phi}2 = \dot{\phi}^2 \quad (23)$$

Assuming independence of all the estimates, the variance of the second-order squares can be expressed as:

$$V(M2_{\phi, \dot{\phi}}^*) = V(M_{\phi2, \dot{\phi}2}^*) + V(V_\phi^*) \cdot V(V_{\dot{\phi}}^*) - (V_\phi^*)^2 \cdot V(V_{\dot{\phi}}^*) - (V_{\dot{\phi}}^*)^2 \cdot V(V_\phi^*) \quad (24)$$

The first term in equation (23) is the variance of the estimate of covariance of the centered squares. It can be calculated using formula (17), but auto- and cross-correlation functions are calculated for the centered squared (22) instead of roll angles and rates. Other terms are variances of the variance estimates of roll angles and rates. Formula for the variance of the variance is available in the literature, Priestley (1981), for example. Details of application of this formula for roll motions are discussed in (Belenky and Weems 2012).

Figure 10 shows the estimates of the second-order coefficients calculated for all four sample data sets. The wave data set has shown independence between the wave elevations and their temporal derivative. This is expected result, because for a normal process, absence of correlation means independence. It also means that the calculation technique is robust enough (despite all the assumptions) to recover the correct theoretical result.

All the ship motion data sets indicate dependence between roll angles and rates. However, the confidence interval of estimate of r2 of the for the beam seas almost “touches” the unity. This may be interpreted that the dependence in beam waves is not that strong. The result in stern quartering seas shows significant dependence between roll angles and rates. These results support the hypothesis expressed above that this dependence may be the results of stability variations in waves that is much stronger in stern quartering seas than in beam seas.

## ELEMENTS OF THE NUMERICAL PROCEDURE

### General

The objective of the numerical procedure is to calculate the probability of capsizing using formula (1) and the results of an advanced numerical code. Following the Principle of Separation, the problem is presented in two parts. The objective of the non-rare problem is to evaluate the upcrossing rates, which can theoretically be presented with formula (10). The objective of the rare problem is to calculate the probability of capsizing after upcrossing, which can theoretically be presented with formula (11). The major component of formula (11) is the distribution of the process  $y$  (the difference between the critical and instantaneous roll rates) at the instant of upcrossing. This distribution provides the interface between the rare and non-rare problem, and its theoretical solution is given by formula (12).

These three computations are the principal elements of the numerical procedure and the objectives of the study described in this section of the paper.

### Rate of Upcrossings

The dependence of the roll angles and rates requires the consideration of the joint PDF of these processes in order to evaluate the upcrossing rate. A direct use of formula (10) for this purpose is impractical because the joint PDF must be evaluated at the upcrossing threshold, and a reliable approximation of the joint PDF can be achieved only if the computed data sample contains a sufficient number of the threshold values. But if it is the case, the upcrossing rate can be estimated by direct counting and the formula (10) is not necessary.

If there are no (or an insufficient number of) upcrossings encountered, the non-rare problem is, in fact, an extrapolation problem of its own. It is, however, simpler than the capsizing probability, because the threshold is much lower and the upcrossing of an angle around the maximum of the GZ curve is significantly less rare than a capsizing.

Belenky and Campbell (2011) reported a comprehensive study of the extrapolation of an estimate of the upcrossing rate. One of the considered methods is Peak-over-Threshold (POT) method, which can be used to characterize the nonlinear response at the upcrossing threshold by further separating the non-rare response at a lower threshold (see also Campbell and Belenky (2010, 2010a). This lower threshold is chosen to be low enough for sufficient upcrossings to be observed, but high enough that the nonlinearity of

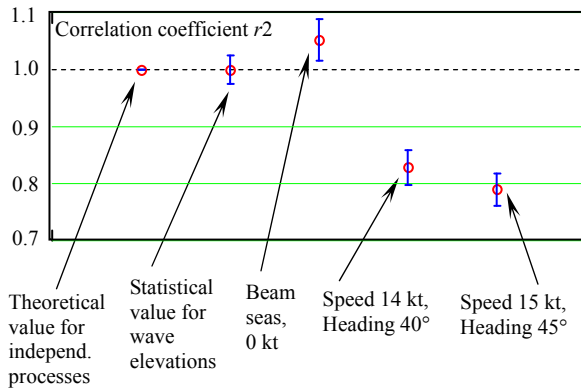


**Figure 10.** Estimates of Second-Order Correlation Coefficient between the Processes and Derivatives (Belenky and Weems 2012a)

### Visual Appearance of Dependence without Correlation

Correlation between two random variables can be visually seen in the joint distribution as a turn of the axis, when looking at horizontal sections, see Figure 11.

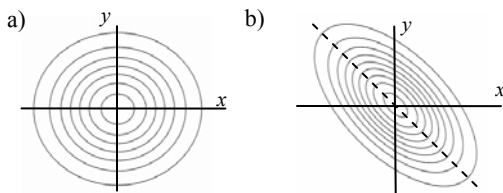


**Figure 12:** Theoretical Gaussian Joint Distributions (a) without and (b) with Correlation

Figure 13 shows graphic representation of joint distribution of roll angles calculated from the stern quartering data set. The moving average method was used to approximate the PDF and reveal its shape. As expected, there is no obvious “turn of the axis” in the horizontal section of joint PDF. However, these sections look a little bit “squeezed” from the diagonal directions. This change from the usual oval shape may be a visual sign of the dependence without correlations.

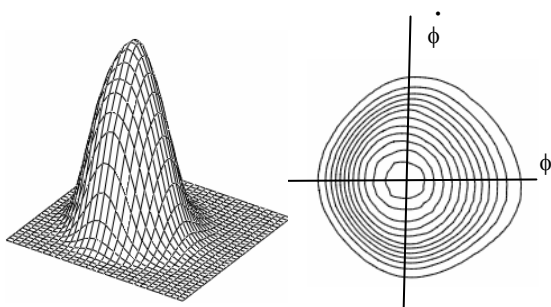


**Figure 13:** Joint Distribution for Heading 45° at 15 Knots (Belenky and Weems 2012a)

the system has already influenced the response and Poisson flow is applicable.

Peaks exceeding this threshold can be sampled using two techniques. The first technique fits a distribution with all the peaks using a Weibull or truncated Raleigh distribution. Then, the rate of upcrossing of the level above the 1<sup>st</sup> threshold can be expressed as:

$$\xi_2^* = -\frac{1}{T_W} \ln(\exp(-\xi_1^* T_W)) + \left(1 - \exp(-\xi_1^* T_W)\right) \frac{F_{EV}(\phi_{m01}, T_W)}{F_{EV}(\phi_{m01}, T_W)} \quad (25)$$

Here  $\phi_{m01}$  the threshold where a sample of sufficient size can be obtained;  $\xi_1^*$  is the statistical estimate of the rate of upcrossing of the 1<sup>st</sup> threshold  $\phi_{m01}$ ; and  $F_{EV}(\phi_{m01})$  is the cumulative distribution function (CDF) of the extreme values exceeding the threshold  $\phi_{m01}$  over a time windows  $T_W$ , see Figure 14.

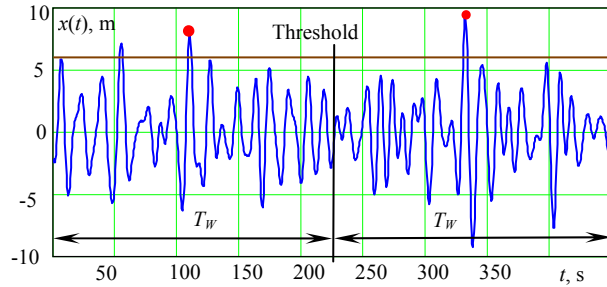


**Figure 14** Sampling for Extreme Value Distribution Fit

The scheme for the calculation of a confidence interval for this estimate is presented in Campbell and Belenky (2010b).

### Extrapolation for Distribution of Dependent Processes

Calculating the probability of capsizing using formula (12) requires a joint distribution of the carrier process  $x$ , the dependent process  $y$ , and the derivative of the process  $z = \dot{x}$ . Fitting such a distribution, while possible, may present a significant challenge, since all three processes may be mutually dependent and not normal. Instead, the following extrapolation scheme may be used:

1. Set a series of the intermediate thresholds of the carrier process  $x$  where upcrossings can be observed in statistically significant numbers
2. Collect a sample of values of the dependent process  $y$  at the instant of each upcrossing
3. Estimate the mean value and variance for each of the intermediate thresholds

4. Fit curves for the mean values and variances as a function of the intermediate thresholds' locations using sample estimates from the previous step
5. Evaluate a histogram for each sample
6. Recalculate all the histograms from the previous step to zero mean value and unity variance
7. Average the histograms from the previous step as an approximation of the distribution
8. Use the fitted curve to extrapolate the mean value and the variance up to the level of interest
9. Use the extrapolated mean value and the variance to recalculate the approximate distribution at the level of interest
10. Attach the tails to the distribution from the previous step, check normalization, and apply formula (11)

The application of this procedure is demonstrated using 200 records of the wave data set (30 minute records generated via a Bretschneider spectrum for Sea State 8 with  $H_S=11.5$  m and  $T_m=16.4$ s). The dependent process was created by applying a phase shift (Belenky *et al.* 2010). Since all of the processes are normal, their dependence is completely defined by the correlation moment, and the “carrier” process  $x(t)$  is truly independent of its derivative. An important aspect of this demonstration is that distribution of the dependent process at upcrossing can be analytically evaluated for any level using formula (12) and provides an exact basis for comparison.

### Mean Value and Variance of Dependent Process

The series of intermediate thresholds consisted of 25 values from 6 to 12 m with a step of 0.25 m. A minimum of 10 values were used to estimate the mean value, and a minimum of 30 values was used for the standard deviation. The results are shown in Figure 15 along with the theoretical values. Both statistical values were fitted with the straight lines using the minimum squares method.

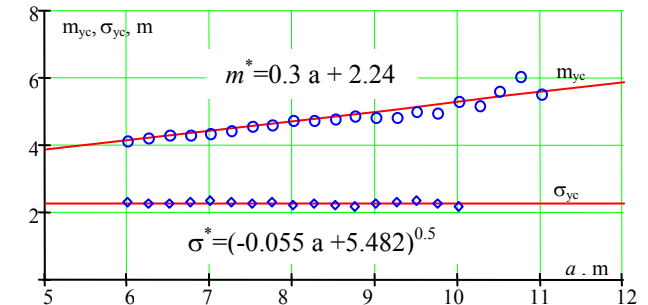


**Figure 15** Statistical Estimates of Mean Values and Standard Deviation Compared to Theoretical Values

### Distribution of Dependent Process

Histograms are evaluated for each intermediate threshold where at least 100 crossings were available. The width of the bin is calculated with Scott's formula (Scott 1979);

$$W(a) = \frac{3.5\sigma_{yc}^*(a)}{\sqrt[3]{N_c(a)}} \quad (26)$$

Here  $\sigma_{yc}^*$  is an estimate of the standard deviation of the dependent process at the upcrossing,  $a$  is the current intermediate threshold for upcrossing, and  $N_c(a)$  is the number of upcrossing over the threshold  $a$ .

All the histograms are then recalculated to zero mean value and unity variance. If the histograms are expressed in terms of probability density, this recalculation is done by changing scale on the abscissa axis:

$$u = \frac{y - m_{yc}^*}{\sigma_{yc}^*} \quad (27)$$

Here  $m_{yc}^*$  is an estimate for mean value of the dependent process at the upcrossing.

The results in Figure 16 clearly show that the theoretical distribution is a mean for the plotted statistical distributions, which are plotted in the form of frequency polygons. Averaging over the statistical distribution reveals the shape of the distribution in Figure 17 that is smooth enough to be used as a model for distribution (using linear interpolation) without further smoothing.

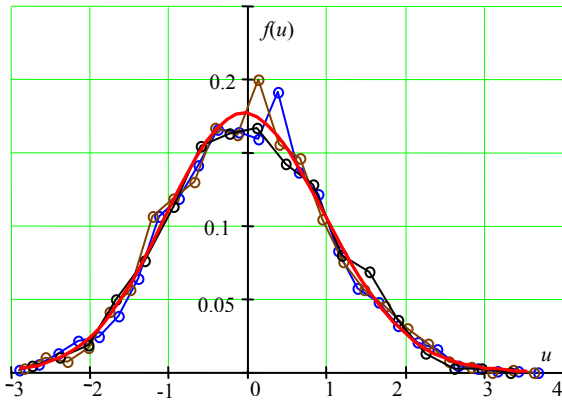


**Figure 16:** Recalculated Statistical Distributions in a Form of Frequency Polygons Superimposed on the Theoretical Distribution (Only Three Polygons are Shown)

The next step is to recalculate the distribution to the values of average and variance extrapolated for the threshold of interest:

$$y_c = u\sigma_{yc}(a) + m_{yc}(a) \quad (28)$$

The sample result for  $a=20$  m is shown in Figure 18. Despite having no statistical data for this level

(maximum observed value for the process  $x$  was 13.83 m), the approximate distribution looks quite reasonable in comparison to the known theoretical distribution.

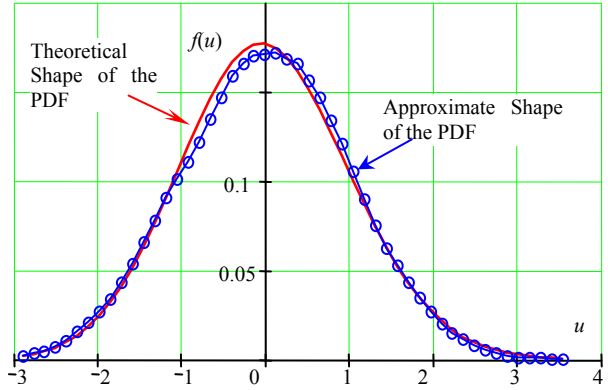


**Figure 17** Theoretical and Approximate Shapes of PDF of the Dependent Process at Upcrossings

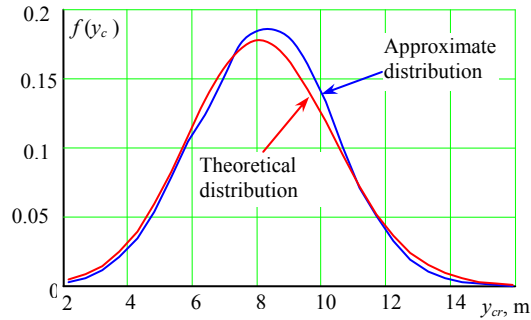


**Figure 18** Approximate and Theoretical Distributions of the Dependent Value at Crossing of the Level of 20m

### Attaching a "Tail"

The problem, however, is that this distribution cannot be used to calculate the probability of the negative values of  $y$  at upcrossing as required in formula (11) since it starts from the value 2.14 m. Thus, one more extrapolation is needed to complete the solution – a tail needs to be attached to the approximate distribution. The tail of the distribution is approximated as

$$f_{tail}(y) = p_1 \exp\left(-\frac{(y-p_2)^2}{p_3}\right) \quad (29)$$

The coefficients  $p_1$ ,  $p_2$  and  $p_3$  are found from the following set of conditions:

- Value of the tail equals the PDF at the chosen attachment point
- The first derivative of the tail at the attachment point equals the PDF derivative at this point
- Minimize the square of the deviation between the tail and the points of the PDF beyond the attachment point (less if negative, more if positive).

The fulfillment of these conditions is expressed as a system of algebraic equations:

$$\left\{ \begin{array}{l} p_1 \exp\left(-\frac{(y_{at} - p_2)^2}{p_3}\right) = f_a(y_{at}) \\ -2p_1 \frac{(y_{at} - p_2)}{p_3} p_1 \exp\left(-\frac{(y_{at} - p_2)^2}{p_3}\right) \\ \qquad \qquad \qquad = \frac{\partial f_a(y)}{\partial y} \Big|_{y=y_{at}} \\ \sum_{i=n_{at}}^{n_{end}} p_1 \frac{(y_i - p_2)^2}{p_3} \exp\left(-\frac{(y_i - p_2)^2}{p_3}\right) \\ \times \left( p_1 \exp\left(-\frac{(y_i - p_2)^2}{p_3}\right) - f_a(y_i) \right) = 0 \end{array} \right. \quad (30)$$

Where  $y_{at}$  is the abscissa of the chosen attachment point,  $f_a$  is the approximate PDF,  $n_{at}$  is an index of the attachment point in the array of the values of  $y_i$  used for defining the approximate PDF, and  $n_{end}$  is the index of the first point in the case of “negative” tail (that tends to negative infinity) or the last point in the case of “positive” tail (that tends to positive infinity).

In the same manner that multiple threshold levels were used with the POT method, it makes sense to create a set of attachment points rather than picking a single value. The result is then averaged in the following way:

$$f_{tail}(y) = \frac{1}{nb(y) - n_{at}} \times \sum_{i=n_{at}}^{nb(y)} p_{1,i} \exp\left(-\frac{(y - p_{2,i})^2}{p_{3,i}}\right) \quad (31)$$

Here  $nb(y)$  is the index of the nearest point from  $\{y_i\}$  to the current point  $y$ . The sample result for the negative tail is shown in Figure 19. The tail was fitted by averaging among four attachment points corresponding to the interval between the 5<sup>th</sup> and 20<sup>th</sup> percentiles.

The final calculation is the probability of encountering a negative value of the process  $y$  when the process  $x$  crosses the level of  $a=20$  m:

$$P_C^* = \int_{-\infty}^0 f_a(y) dy = 1.33 \cdot 10^{-4} \quad (32)$$

$$P_C = \int_{-\infty}^0 f_c(y) dy = 0.65 \cdot 10^{-4}$$

Here  $P_C^*$  is an extrapolated value, while  $P_C$  is the theoretical value. Keeping in mind that the rate of upcrossing at the level of 20 m is on the order  $10^{-13}$ , the considered event has a rate on the order of  $10^{-17}$ . An error

of about 100% seems like a very accurate result for such a rare event, which demonstrates the practicality of the proposed method.

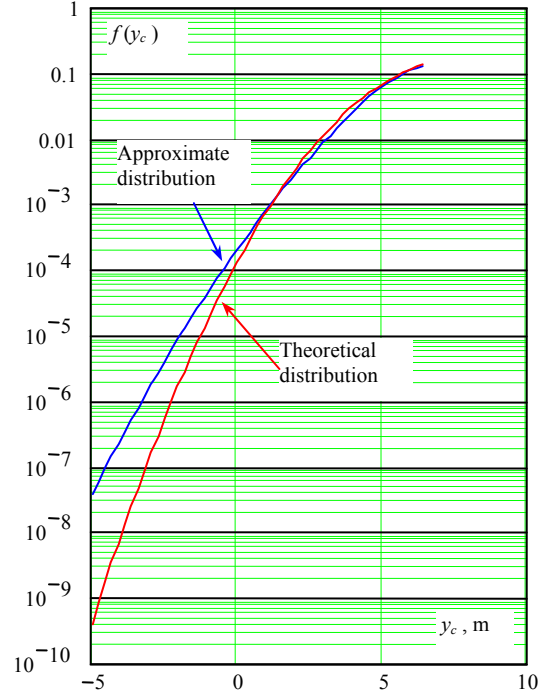


**Figure 19:** Comparison of Approximate Negative Tail Averaged Among 4 Attachment Points, Corresponding to Range from 5<sup>th</sup> to 20<sup>th</sup> Percentile

## MODEL OF SURGING IN IRREGULAR WAVES

### General

As was noted above, the dynamics of surf-riding and broaching-to in regular waves is well understood (Spyrou 1996, 1997) and the physics of these phenomenal can be well reproduced by advanced hydrodynamic codes (Spyrou *et al.* 2009). This creates a solid background for the development of probabilistic methods, especially those that use the Principle of Separation of system dynamics. Themelis and Spyrou (2007) successfully applied the critical wave groups method to estimate the probability of stability failures in waves, that can handle the broaching-to instability. The strength of the wave group method is its flexibility in terms of the selected level of rigor, thus allowing practicality in different contexts. The split-time method, on the other hand, may be more robust in terms of reflecting the statistics of initial conditions. Since the methods share the same philosophy of handling rarity (Belenky *et al.* 2012), they have a potential to complement each other. The application of a probabilistic method for surf-riding and broaching-to encounters a challenge that was not present before: the

necessity to consider the problem in time and space in the same time.

A cornerstone of the dynamics of surf-riding is the appearance of a pair of surf-riding equilibria of which the one that attracts in surge may be a repeller in yaw, depending on the effectiveness of rudder control. Another key issue is the possible dominance in state space of this equilibrium due to a “homoclinic connection” bifurcation that renders surf-riding inevitable. For this reason, the analysis of the probabilistic properties of the equilibrium in irregular way is the next objective (Belenky *et al.* 2011a, 2012a; Spyrou *et al.* 2012).

### Physics of Surf-Riding

The physical mechanism of surf-riding includes the appearance of dynamical equilibria and a ship’s attraction to the stable equilibrium. The equilibria appear when the wave surging force becomes large enough to offset the difference between the ship’s thrust and its resistance at wave celerity. The equilibrium points are the positions of the ship on the wave where the forces balance exactly.

To illustrate this, consider surf-riding in regular waves and plot the variation in the wave-induced surging force as a function of the ship’s position on the waves; see Figure 20. In this plot, the horizontal axis is the position of the ship’s center of gravity ahead of the wave crest, the dashed blue line is the wave profile, and the red line is the wave surging force, with a negative value indicating a forward (accelerating) force. The largest forward surging force (most negative on this plot) occurs when the ship is running down the wave face. The magnitude of surging force is a function of wave amplitude.

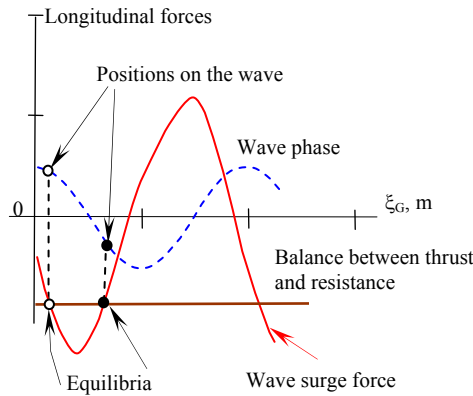


**Figure 20** On the Appearance of Surf-Riding Dynamic Equilibria (Belenky *et al.* 2012a)

Since the commanded rpm is insufficient to propel the ship with wave celerity even in calm water, additional wave force is necessary to drive the ship at

wave celerity. If the amplitude of the wave surging force exceeds the absolute value of the balance between thrust and resistance, two intersection points appear, as shown in Figure 20. Those will be called “surf-riding equilibria” (though it is known that this is not an exact condition of equilibrium); one shows stable features (black point, located around the wave trough) and the other behaves unstably (empty point, located around wave crest).

### Equation of Motion

Consider a simple model for one-degree-of-freedom nonlinear surging:

$$(M + A_{11})\ddot{\xi}_G + R(\dot{\xi}_G) - T(\dot{\xi}_G, n) + F_X(t, \xi_G) = 0 \quad (33)$$

Here  $M$  is mass of the ship,  $A_{11}$  is longitudinal added mass,  $R$  is resistance in calm water,  $T$  is the thrust in calm water,  $n$  is the number of propeller revolutions,  $F_X$  is the Froude-Krylov wave surging force, and  $\xi_G$  is longitudinal position of the center of gravity in the Earth-fixed coordinate system. The dot above the symbol stands for temporal derivative.

Polynomial presentations are used for the resistance and thrust:

$$\begin{aligned} R(U) &= r_1 U + r_2 U^2 + r_3 U^3 \\ T(U, n) &= \tau_1 n^2 + \tau_2 n U + \tau_3 U^2 \end{aligned} \quad (34)$$

The coefficients  $r$  and  $\tau$  are meant to be fit to the appropriate calm water curves (Spyrou 2006).

### Wave Surging Forces

Since the Earth-fixed coordinate system is used, irregular waves are presented as a spatial–temporal stochastic process using the standard Longuet-Higgins model:

$$\zeta_W(t, \xi) = \sum_{i=1}^N r_{Wi} \cos(k_i \xi - \omega_i t + \varphi_i) \quad (35)$$

$\xi$  is the spatial coordinate,  $r_{Wi}$  is amplitude of the wave component characterized by the wave number  $k_i$  and frequency  $\omega_i$ ; and  $\varphi_i$  is a random phase with uniform distribution from 0 to  $2\pi$ . The dispersion relation connects the wave number and frequency of each component.

$$k_i = \frac{\omega_i^2}{g} \quad (36)$$

Here  $g$  is the gravity acceleration. As the model is meant at this stage to be qualitative, a linear wave-body formulation seems to be appropriate, so:

$$F_X(t, \xi_G) = \sum_{i=1}^N A_{Xi} \cos(k_i \xi - \omega_i t + \varphi_i + \gamma_i) \quad (37)$$

As a body-linear formulation is adopted, the amplitude  $A_{X_i}$  and phase shift  $\gamma_i$  are available from the response amplitude and phase operators:

$$A_{X_i} = r_{w_i} RAO(k_i) \quad (38)$$

$$RAO(k_i) = \rho g k_i \left( \left( \int_{-0.5L}^{0.5L} C(x, k_i) \cos(k_i x) dx \right)^2 + \left( \int_{-0.5L}^{0.5L} C(x, k_i) \sin(k_i x) dx \right)^2 \right)^{1/2} \quad (39)$$

$$C(x, k_i) = 2 \int_{-d}^0 \exp(k_i z) b(x, z + d) dz \quad (40)$$

$$\gamma_i = \arctan \left( \frac{\int_{-0.5L}^{0.5L} C(x, k_i) \sin(k_i x) dx}{\int_{-0.5L}^{0.5L} C(x, k_i) \cos(k_i x) dx} \right) \quad (41)$$

Here  $x$  and  $z$  are measured in the ship fixed coordinate system (positive forwards of amidships and upward from the base line),  $b(x, z)$  is the molded local half-breadth and  $d$  is the amidships section draft.

Figure 21 shows the RAO of the surging wave force for the tumblehome ship from the ONR topside series (Bishop *et al.* 2005). The phase shift  $\gamma_i$  is presented as Figure 22.

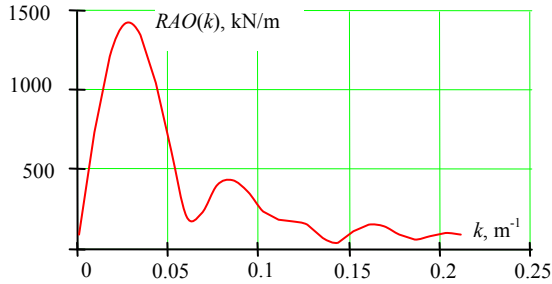


**Figure 21:** RAO of Surging Force (Belenky *et al.* 2011a)

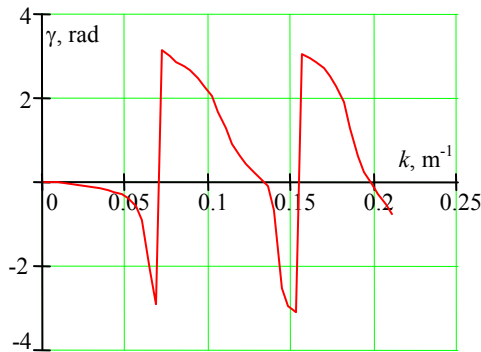


**Figure 22:** Phase Shift of Surging Force (Belenky *et al.* 2011a).

## Wave Bandwidth

Belenky *et al.* (2011a) used a variable bandwidth for irregular waves to see the effect of irregularity by increasing number of frequency components. A filter was used for this purpose:

$$F(\omega_i) = \begin{cases} 0 & \omega < b_{low} \Delta \omega \\ \frac{\omega - \omega_m - b_{low} \Delta \omega}{b_{low} \Delta \omega} & b_{low} \Delta \omega \leq \omega < \omega_m \\ \frac{\omega - \omega_m + b_{up} \Delta \omega}{b_{low} \Delta \omega} & \omega_m \leq \omega \leq b_{up} \Delta \omega \\ 0 & \omega > b_{up} \Delta \omega \end{cases} \quad (42)$$

Here  $\omega_m$  is the modal frequency of the spectrum while  $\Delta \omega$  is the frequency step. The filter consists of two lines: the low frequency corresponds to the index  $b_{low}$  and the high frequency index is  $b_{up}$ . These two indices are parameters for controlling the spectrum bandwidth. To keep the variance of the wave elevation constant, a normalization coefficient is used:

$$K_N = \frac{\sum_{i=1}^N a_i}{\sum_{i=1}^N a_i F(\omega_i)} \quad (43)$$

A sample result of the bilinear filter is shown in Figure 22. After discretizing a Bretschneider spectrum with 174 frequencies, a total filtered spectrum is created by selecting the lower boundary 10 frequencies below the modal frequency and the upper boundary 20 frequencies above the modal frequency. This corresponds to a decrease of the spectrum bandwidth parameter from 0.703 to 0.21

Using the filter (42) and the model (33) allowed Belenky *et al.* (2011a) to study the influence of the bandwidth on the surf-riding. It was found that it enough to have only two frequency component to observed a “catch and Release” *i.e.* surf-riding for a finite duration of time. This is a principle difference between surf-riding in regular and irregular waves.

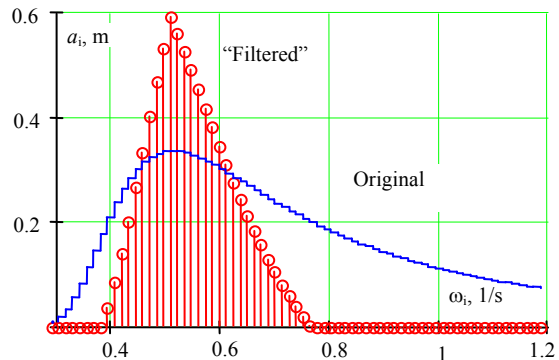


**Figure 23:** Example of Changing Wave Spectrum Bandwidth Using a Filter (Belenky *et al.* 2011a).

## CELERITY OF IRREGULAR WAVES

A phenomenological approach to surf-riding prediction would use wave celerity as the threshold ship speed that, if surpassed, would realize an attraction to surf-riding. However, the definition of celerity for an irregular sea might be contemplated in more than one way, each of which may produce quantitatively different values. By any definition, celerity is not necessarily a smooth curve and it can contain jumps to infinity which cannot be tolerated in an ordinary surf-riding assessment framework. Therefore, the handling of irregular wave celerity is an important milestone on the way toward establishing a rational approach.

Longuet-Higgins (1957) and more recently Baxevani *et al.* (2003), Aberg and Rychlik (2007) and others have produced distributions for various wave velocities of a Gaussian sea. However, a key difficulty of a formulation targeting surf-riding prediction is that it is based on a process built from the difference between celerity and ship speed which is strongly nonlinear when surf-riding is about to happen. Therefore, a statistical model of celerity alone cannot be used. Various ideas on a proper definition of a localized in time-space celerity for the problem at hand are found in Spyrou *et al.* (2012). It was considered as quite relevant to monitor the velocity of the steepest point on the down slope of the wave profile that is nearest to the ship. The maximum wave force in surge (which is known to be a critical factor for surf-riding) presents usually only a small difference in phase from the wave slope. At least one such point can always be identified on the down slope of every apparent cycle. Whilst it can degenerate to zero slope when its distance from a neighboring crest or trough shrinks to a zero length, such wave encounters represent relatively mild conditions for the ship and such singular points should therefore be unimportant for the surf-riding probability calculation.

Let  $\xi_G(t)$  be the ship's position at some arbitrary time instant  $t$ . The following equation (44) can be solved numerically for  $x_{a_{\max}} = f(t, a_{\max})$  in order to identify points of maximum slope near to the ship :

$$\frac{\partial^2 \zeta(x_{a_{\max}}, t)}{\partial x^2} = 0 \quad (44)$$

$\zeta$  and  $x$  are, respectively, the elevation and the longitudinal location of a considered point of the wave profile. Newton iterations to find this are started from the ship position  $\xi_G(t)$ . To ensure that the point is on the down slope, the following inequality is simultaneously checked:

$$\frac{\partial^3 \zeta(x_{a_{\max}}, t)}{\partial x^3} < 0 \quad (45)$$

For a finite difference approximation of the derivative, additional points need to be determined, separated by a small time interval  $\delta t$ .

$$\frac{\partial^2 \zeta(x_{a_{\max}}, t + k \cdot \delta t)}{\partial x^2} = 0$$

↓

$$x_{a_{\max}}^{(k)} = f(t + k \cdot \delta t; a_{\max}) \quad (46)$$

To be certain that the located points lie near the ship, one additional inequality condition can be imposed on the solution  $x_{a_{\max}}^{(k)}$  :

$$\left| x_{a_{\max}}^{(k)} - \xi_G(t) \right| < d \quad (47)$$

As an appropriate value of  $d$  one can obtain some ratio of the instantaneous wave length (e.g. 30%).

A demonstration of this calculation method is shown below for the Topsides tumblehome ship traveling in bi-chromatic waves. In Figure 24 the surge response reaches just below the celerity curve and the ship responds in an ordinary quasi-periodic manner. It is noted that although the peak of the ship's speed response exceeds the celerity of the shorter wave (green line), no major effect comes about. However, as shown in Figure 25, a slight increase of the calm water speed (propulsion force) creates an up-crossing of the time-varying celerity curve and capture into an oscillatory type of surf-riding with significant departures from the celerity speed. In this case, the presented celerity curve seems to be suitable to serve the role of the threshold speed curve for surf-riding. Further examples including multi-frequency cases can be found in Spyrou *et al.* (2012) Following its initial verification using the 1-DOF model of surging, the irregular wave celerity calculation is being implemented in the Large Amplitude Motions Program (LAMP). The LAMP implementation of the wave celerity calculation generally follows the scheme described above, but has been adapted for LAMP's more general irregular wave models including oblique, short-crested (multi-direction) and nonlinear incident waves. The wave point that is tracked is the maximum wave slope in the direction of ship travel; it is tracked only in that direction, and the resulting wave celerity is calculated in this direction.

In the LAMP implementation of the wave celerity calculation is always searched for the nearest maximum slope point on the down slope even if an up slope maximum is closer. This is done by pre-computing the elevation and its derivatives on a regular spatial interval  $\delta x_s$  in the travel direction and identifying intervals where a down-slope maximum can be found.

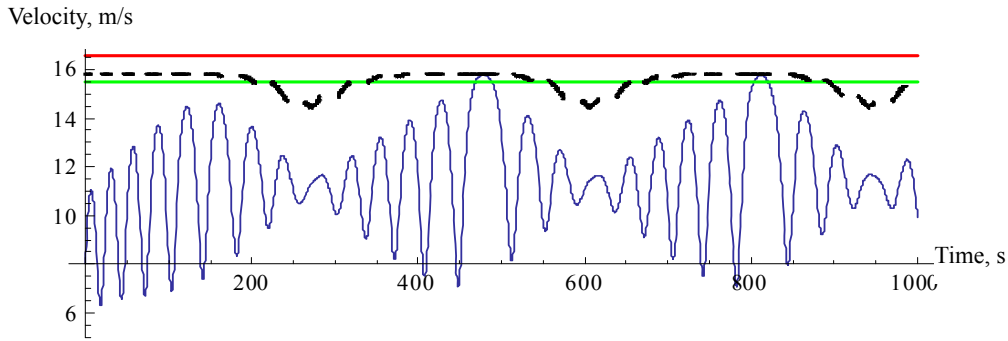


**Figure 24:** A surging pattern in a bichromatic sea just before surf-riding ( $Fn=0.28$ ):  $\zeta_1=2.5$  m,  $\lambda_1=175$ m and  $\zeta_2=3.4$ m,  $\lambda_2=152$ m. The straight lines indicate the celerities corresponding to the two harmonic wave components. The broken line is the calculated celerity curve (Spyrou *et al.* 2012).

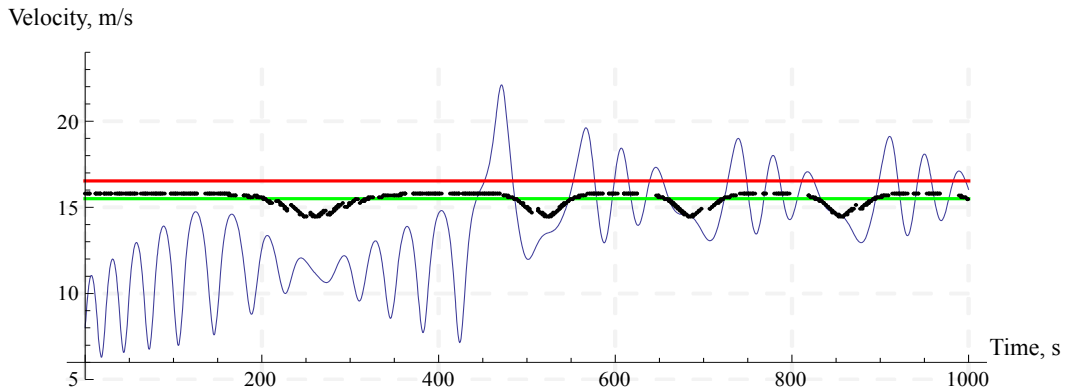


**Figure 25:** As the celerity threshold is surpassed by slightly increasing the  $Fn$  value to 0.283, surf-riding appears (Spyrou *et al.* 2012).

Figure 26 shows a snapshot of a LAMP simulation for the tumblehome hull form from the ONR Topsides series running in long-crested irregular waves. The plot shows the wave profile at that time instance along the ship's travel direction with marks for the points of maximum down slope and elevation (crest). The wave in this case is derived from a Bretschneider spectrum with  $H_S=7$ m and  $T_m=12.0$ s

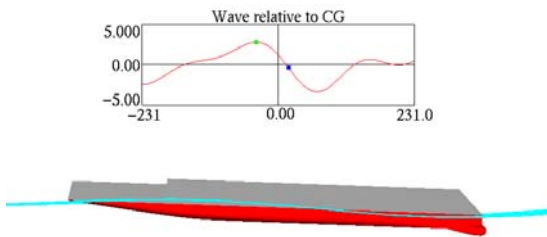


**Figure 26** LAMP simulation of ONR Topsides tumblehome hull in irregular following seas.

### SURF-RIDING EQUILIBRIA IN IRREGULAR WAVES

The patterns of surf-riding in irregular waves have been discussed already in Belenky *et al.* (2011, 2012) and Spyrou *et al.* (2012). A question that underlies these studies is: how is the surf-riding behavior related with the appearance or disappearance of surf-riding equilibrium?

A preliminary attempt to answer this question is given below. A time history for an example with three-component wave from Belenky *et al.* (2012) is presented in Figure 27a. This example was chosen because it contains two “catches” and one “release”, as well as obvious asymmetric surging. The importance of the latter is that the asymmetric surging is related to the presence of surf-riding equilibrium (Spyrou, 2006).

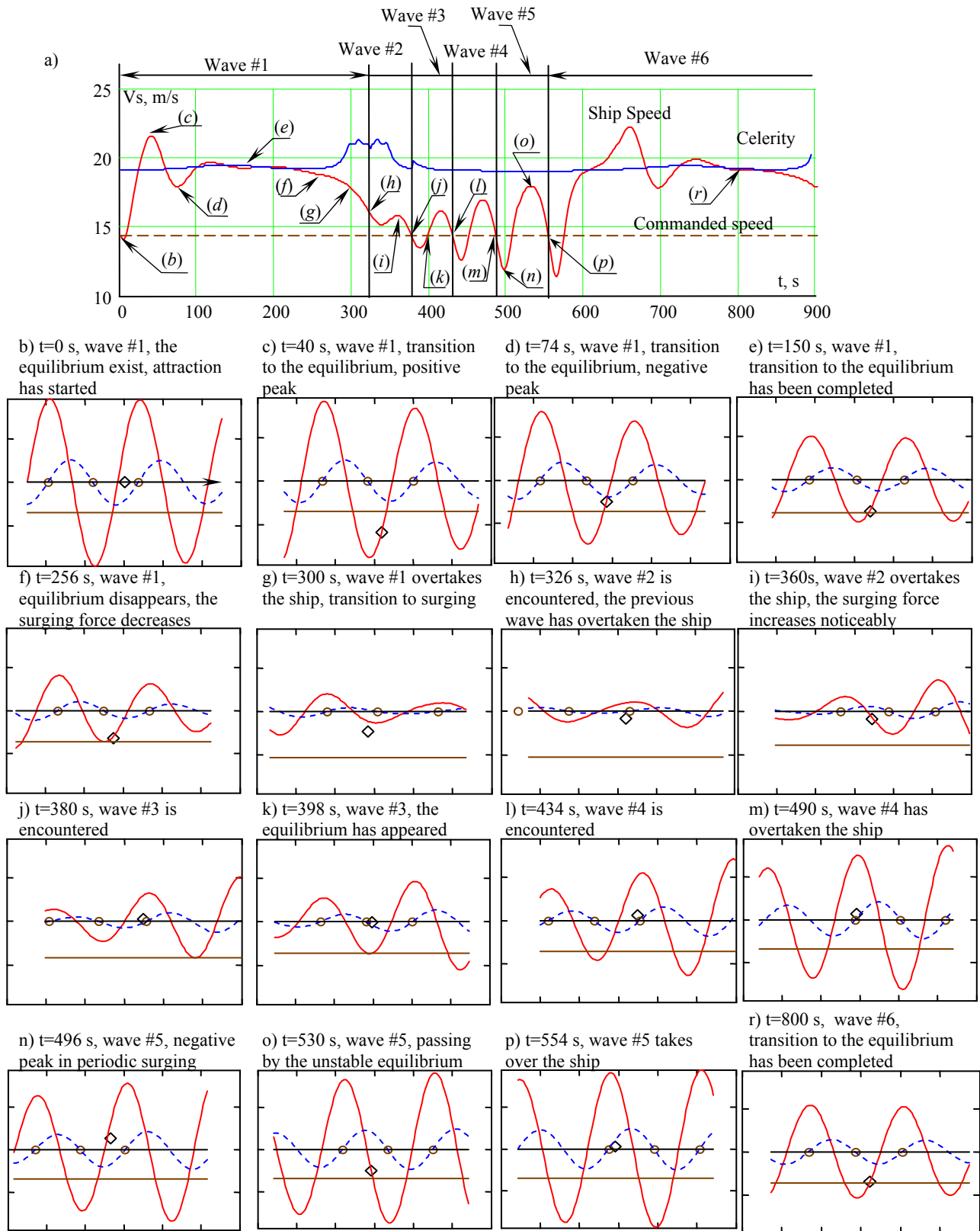


**Figure 27** Two captures and one release from surf-riding in a three-component irregular wave; time history (a) and “spatial snapshots” (b-r) (Belenky *et al.* 2012)

The duration of the sample case is 15 minutes. During that time six waves overtake the ship. The time instances when one wave passed and another one was encountered are shown in Figure 27a. Following the definition described in the previous section, the celerity was determined by the “current” wave and was based on zero-crossing points.

The rest of Figure 27 are “spatial snapshots” (b through r). Each of these snapshots describes a “spatial picture” corresponding to a particular instant of time identified in Figure 27a with arrows. The content of each snapshot is analogous to Figure 20; it contains the wave phase, the “spatial history” of the wave surging force and the line corresponding to the balance between the resistance and thrust. The intersections of the wave force and the balance line represent an approximation of the equilibria (strictly speaking, the inertial force is no longer zero since the wave celerity is no longer a constant). In addition, each spatial snapshot also has the boundaries of the “current wave” (in the form of the zero-crossing points) as well as a diamond marking the position of a ship. The abscissa of the diamond shows ship’s position relative to the wave phase. The vertical coordinate corresponds to the total force; so when the diamond is located on the intersection of the force curve and the balance line, it means that the equilibrium has been achieved at this instant.

The first spatial snapshot, Figure 27b, corresponds to the initial conditions, with the instantaneous speed equal to the commanded (calm water) speed. The ship has just encountered wave #1 and is located just within its boundary. The surf-riding equilibria exist since the surging force crosses the line corresponding to the balance between the thrust and resistance.

The stable surf-riding equilibrium attracts the dynamical system and one oscillation period is seen in Figure 27a until approximately  $t=100$ s. The next two spatial snapshots, Figures 27c and 27d, correspond to the positive and negative peaks during this transition, respectively. The transition is completed and the dynamical system reaches the stable surf-riding equilibrium at around  $t=150$  s, in Figure 27e.

Looking at Figures 27b through 27e, one can see that the amplitude of the surging force is decreasing due to lower wave amplitude. This tendency leads to the disappearance of the surf-riding equilibria around  $t=256$  s and the release of the ship from surf-riding (Figure 27f).

The ship slows down (Figure 27g), then wave #1 overtakes her, and wave #2 is encountered at around  $t=325$  s (Figure 27h). The ship experiences the first almost periodic surge with the positive peak corresponding to the spatial snapshot in Figure 27i. As expected, wave #2 overtakes the ship quite quickly and wave #3 is encountered around  $t=380$  s (Figure 27j)

The modulation of wave amplitude and surging force then reverses and they begin to increase. This is may be already seen in Figure 27h, but becomes quite apparent in Figures 27i and 27j. New surf-riding equilibria appear around  $t=398$  s (Figure 27k).

The existence of the surf-riding equilibria has an immediate influence on the surge motions, which become asymmetric with wider positive peaks and sharper negative ones (Spyrou, 2006). Symmetry is observed during the passing of waves #4 and #5, during which the surf-riding equilibria exists continuously (Figures 27l through 27o). Figure 27o shows how the dynamical system passed near the unstable surf-riding equilibrium, but the ship is not yet “caught” and wave #5 takes over (Figure 27p). The ship is finally “caught” by wave #6 and at around  $t=800$  again reaches the stable surf-riding equilibrium (Figure 27r).

The detailed study of this example reveals the existence or non-existence of the surf-riding equilibria, which could then be used to explain the ship’s transition into and out of surf-riding in irregular seas. This ability to characterize the behavior of the dynamical system from these equilibria allows consideration of a probabilistic formulation for surf-riding in irregular waves.

## CONCLUSIONS AND FUTURE WORK

The paper describes the background and current status of ongoing research on the probability of capsizing in irregular seas. The overall objective of the project is to evaluate the probability of capsizing or a large roll angle event with the split-time method. The main idea of split-time method is to separate the difficult problem of capsizing probability into two problem of more manageable complexity: a non-rare related to the upcrossing of the intermediate threshold and a rare problem related to capsizing after the threshold has been crossed. Two modes of stability failure are being considered in the current phase of the project: pure loss of stability and broaching-to preceded by surf-riding.

For capsizing caused by stability variations in waves, the focus has been on numerical implementation issues, as the theoretical “proof of concept” has been successfully completed and previously reported. The probabilistic properties of roll motion in stern quartering seas were studied using the results of LAMP numerical simulation tumblehome configuration of the ONR Topsides series. The results have shown that the dependence between roll angles and rates is significant and cannot be ignored.

The procedure of application of the split-time method was changed accordingly. Instead of using approximations for distributions, the emphasis has shifted to statistical extrapolation methods. While

peak-over threshold (POT) method is used for the rare problem, a special extrapolation method was developed for the distribution of the dependent process at the instant of upcrossing. Application of this method will help to complete the rare problem.

For the probability of capsizing caused by broaching-to, the results of numerical study of surf-riding in irregular waves are reported. A simple, 1-DOF model of surging and surf-riding in irregular waves has been presented that is capable of reproducing the fundamentals of surf-riding behavior in irregular waves.

The consideration of the probabilistic modeling of surf-riding has led to the formulation of the problem of celerity of irregular waves. While this problem is quite deep and goes beyond its application for surf-riding in irregular waves, a satisfactory definition has been derived through the speed of translation of certain wave properties, in particular the maximum of the wave slope. It was also shown that the concept of irregular wave celerity reveals the random appearance and disappearance of the surf-riding equilibria that define the topology of the phase space.

The immediate future work includes the competition of numerical scheme for probability of capsizing caused by stability variation in waves, including research and implementation of uncertainty estimates of the distribution of the dependent process at the instant of upcrossing. For the broaching-to, the future work includes development of scheme of application of the split-time method for surf-riding and broaching-to as well as the test of the concept.

## ACKNOWLEDGEMENTS

The work described in this paper has been funded by the Office of Naval Research under Dr. Patrick Purtell and by ONR Global under Dr. Richard Vogelsong. This support is gratefully acknowledged by the authors.

The authors are grateful to Dr. N. Themelis (National Technical University of Athens) for his calculations regarding the celerity of irregular waves. Discussions with B. Campbell, Dr. A. Reed (David Taylor Model Basin, NSWCCD), Prof. P. Spanos (Rice University) and Prof. M. R. Leadbetter have been very fruitful.

## REFERENCES

Aberg, S. and Rychlik, I. (2007) "Doppler shift approximations of encountered wave statistics," Ocean Engineering, Vol. 34, 2300-2310.

Baxevasani, A., Podgórski, K. and Rychlik, I. (2003) "Velocities for moving random surfaces", Probabilistic Engineering Mechanics, Vol. 18, 251-271.

Belenky, V. L. (1993) "A Capsizing Probability Computation Method," J. Ship Research, Vol. 37, pp. 200- 207.

Belenky, V. and Weems, K.M. (2008) "Procedure for Probabilistic Evaluation of Large Amplitude Roll Motions," Proc. of the Osaka Colloquium on Seakeeping and Stability of Ships, Osaka, Japan.

Belenky, V., Weems, K., M. and W.-M. Lin (2008) "Numerical Procedure for Evaluation of Capsizing Probability with Split Time Method", 27th Symposium on Naval Hydrodynamics, Seoul, Korea.

Belenky, V. and Weems, K.M., (2008a) "Probabilistic Qualities of Stability Change in Waves", Proc. 10th Int. Ship Stability Workshop, Taejon, Korea.

Belenky, V.L., Weems, K.M., Lin, W.M., Spyrou, K.J., (2010), "Numerical Evaluation of Capsizing Probability in Quartering Seas with Split Time Method," Proceedings of 28<sup>th</sup> Symposium on Naval Hydrodynamics, Pasadena, California, USA.

Belenky, V., Campbell, B. (2011). Evaluation of the Exceedance Rate of a Stationary Stochastic Process by Statistical Extrapolation Using the Envelope Peaks over Threshold (EPOT) Method, Naval Surface Warfare Center Carderock Division Report NSWCCD-50-TR-2011/032, 216 p.

Belenky, V., Reed, A.M. and Weems K. M. (2011) "Probability of Capsizing in Beam Seas with Piecewise Linear Stochastic GZ Curve," Contemporary Ideas on Ship Stability, Neves, M.A.S. *et al.* (eds), Springer, pp. 531-554

Belenky, V., Spyrou, K. J., and Weems, K. M., (2011a), "Split-Time Method for Surf-Riding and Broaching-To," Proceedings of 12th International Ship Stability Workshop, (ISSW 2011), Washington DC, pp.163-168.

Belenky, V. Weems, K.M. (2012), "Probabilistic Properties of Parametric Roll" in Parametric Resonance in Dynamical Systems, Fossen, T. I.; Nijmeijer, H. (Eds.) Springer

Belenky, V., Weems, K. (2012a) "Dependence of Roll and Roll Rate in Nonlinear Ship Motions in Following and Stern Quartering Seas", Proc. of 11<sup>th</sup> Intl. Conf. on Stability of Ships and Ocean Vehicles (STAB'2012), Athens, Greece.

Belenky, V., Weems, K., Bassler, C., Dipper, M.J., Campbell, B., Spyrou, K.J. (2012), "Approaches to Rare Events in Stochastic Dynamics of Ships," Probabilistic Engineering Mechanics, Vol. 28, pp. 30–38

- Belenky, V., Spyrou, K. J., and Weems, K. M., (2012a), "Evaluation of the Probability of Surf-Riding in Irregular Waves with the Time-Split Method" Proc. of 11<sup>th</sup> Intl. Conf. on Stability of Ships and Ocean Vehicles (STAB'2012), Athens, Greece.
- Bishop, R. C., W. Belknap, C. Turner, B. Simon, J. H. Kim (2005) Parametric Investigation on the Influence of GM, Roll damping, and Above-Water Form on the Roll Response of Model 5613. Report NSWCCD-50-TR-2005/027.
- Campbell, B., and V. Belenky (2010). "Assessment of Short-Term Risk with Monte-Carlo Method," Proc. of the 11th Int. Ship Stability Workshop, Wageningen, The Netherlands.
- Campbell, B., and V. Belenky (2010a). "Statistical Extrapolation for Evaluation of Probability of Large Roll", Proc. of 11th Int. Symp. On Practical Design of Ships and Other Floating Structures, Rio-de-Janeiro, Brazil.
- Iskandar, B.H., Umeda, N. (2001). "Some Examinations of Capsizing Probability Calculation for an Indonesian Ro-Ro Passenger ship in Waves", Journal of Kansai Society of Naval Architects, No. 236 (September), pp 81-86.
- Longuet-Higgins, M.S. (1957) "The Statistical Analysis of a Random, Moving Surface", Philosophical Transactions of the Royal Society of London. Series A, Mathematical and Physical Sciences, Vol. 249, 966, 321-387.
- Paroka, D., Umeda, N. (2006). "Capsizing Probability Prediction for a Large Passenger Ship in Irregular Beam Wind and Waves: Comparison of Analytical and Numerical Methods," Journal of Ship Research, Vol. 50, No. 4, pp. 371-377.
- Paroka, D., Y. Okura, and N. Umeda (2006), "Analytical Prediction of Capsizing Probability of a Ship in Beam Wind and Waves", J. Ship Research, Vol. 50, No. 2, pp. 187-195.
- Priestley, M. B., (1981), Spectral Analysis and Time Series, Vol. 1, Academic Press, New York
- Scott, D.W. (1979). "On Optimal and Data-based Histograms," Biometrika, 66(3):605-610.
- Spyrou, K.J. (1996) Dynamic instability in quartering seas: The behavior of a ship during broaching, J Ship Research, 1996, Vol. 40, No 1, 46-59.
- Spyrou, K. (1997) "Dynamic instabilities in quartering seas – part III: nonlinear effects on periodic motions", J Ship Research, Vol. 41, No 3, pp. 210-223.
- Spyrou, K.J. (2006), "Asymmetric Surging of Ships in Following Seas and its Repercussions for Safety," Nonlinear Dynamics, Vol. 43, pp. 149-172.
- Spyrou, K. J., Weems, K. M., Belenky, V. (2009) "Verification Of The Patterns Of Surf-riding And Broaching By An Advanced Hydrodynamic Code," Proc. of the 10th Int. Conference on Stability of Ships and Ocean Vehicles, St. Petersburg, Russia
- Spyrou, K. J. , Belenky, V, Themelis, N. Weems, K.M. (2012) "Conditions of Surf-riding in an Irregular Seaway, Proc. of 11<sup>th</sup> Intl. Conf. on Stability of Ships and Ocean Vehicles (STAB'2012), Athens, Greece.
- Themelis, N., and Spyrou, K.J., 2007, "Probabilistic assessment of ship stability," Transactions, SNAME, Vol. 115, pp. 181-206.
- Umeda, N., S. Koga, J. Ueda, E. Maeda, I. Tsukamoto & D. Paroka 2007 Methodology for Calculating Capsizing Probability for a Ship under Dead Ship Condition, Proc. 9th Int'l Ship Stability Workshop, Hamburg, pp. 1.2.1-1.2.19.
- Umeda, N., Izawa, S. Sano, H., Kubo, H., Yamane K. Matsuda, A. 2011 "Validation Attempts on Draft New Generation Intact Stability Criteria" Proc. 12<sup>th</sup> Int'l Ship Stability Workshop, Washington, pp 19-26